ChemComm

Accepted Manuscript

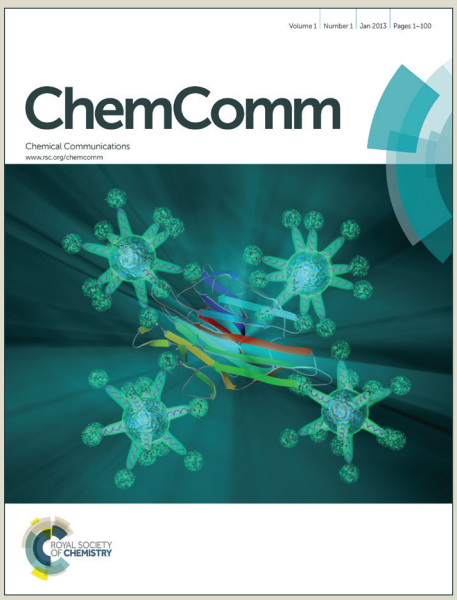

ROYAL SOCIETY OF CHEMISTRY

www.rsc.org/chemcomm

Eggplant-Derived Microporous Carbon Sheets: Towards Mass Production of Efficient Bifunctional Oxygen Electrocatalyst at Low Cost for Rechargeable Zn-Air Batteries

Bing Li,[a#] Dongsheng Geng,[a#] Shannon Lee,[b#] Xiaoming Ge,[a] Jianwei Chai,[a] Zhijuan Wang,[a] Jie Zhang,[a] Zhaolin Liu,[*a] T. S. Andy Hor,[*ac] and Yun Zong[*a]

Received (in XXX, XXX) Xth XXXXXXXXX 20XX, Accepted Xth XXXXXXXXX 20XX
DOI: 10.1039/b000000x

We report 2D microporous carbon sheets with high surface area, derived from eggplant via simple carbonization and KOH activation, as low cost yet efficient bifunctional catalyst for high performance rechargeable zinc-air batteries.

With fast-increasing energy demands and growing concerns on fossil fuel associated environmental issues, interest in developing sustainable and renewable energy sources and high performance energy storage systems have been surging in recent years.[1] Zn-air batteries (ZnABs) emerge as an attractive option of solution because of its environmental benignity and the high theoretical energy density up to 1086 Wh/kg which is about 5 times as high as that of current Li-ion technology.[1a, 1b, 1d, 1i, 2] In addition, the abundance of Zn with its mild reactivity and non-flammability make ZnABs a safe and cost-effective chioce.[1a, 1b] To maintain the cost competitive advantages over other battery technologies, low cost yet efficient catalysts for the air cathode to promote oxygen reduction reaction (ORR) and oxygen evolution reaction (OER) in discharge and charge processes, play a critical role.

As benchmark catalyst platinum (Pt) and Pt alloys have more or less accomplished their mission.[3] The lower cost alternatives, i.e. transition metal oxides[1d, 4] and their composites,[5] however, still face sustainability and cost issues caused by fast depletion at high demand apart from additional concerns of the possible negative impacts on the environment. Moreover, many metal-containing catalysts often tend to agglomerate or detach from the electrode surfaces over time, leading to degradation of their catalytic activity.[1d, 6] These issues are partially solved in some metal-free low-dimension carbon materials, e.g. nitrogen-doped carbon nanotubes[1c] and graphene.[7] However, the preparation of such materials is often tedious and involves toxic chemicals or expensive hardwares,[1c, 7] making them unsuitable for applications with large quantity of materials demand, such as in grid-scale power storage and electric vehicles (EVs).

Nature provides a wide range of plants in high abundance as inexpensive, renewable and entirely green carbon precursors. Upon conversion to unique carbon materials with features of high specific surface area and excellent electrical conductivity,[1e, 8] they are used in electrodes of supercapacitors,[8h, 8i] Li-ion batteries,[1e, 8a] and Na-ion batteries.[8a] Such materials are less known for their electrochemical catalytic activities, e.g. toward ORR and OER,[8c, 8h] with no application in ZnABs being exploited so far. Herein, we demonstrate eggplant as a renewable, high yield and natural starting material for the production of additive-metal-free and highly active electrocatalyst for rechargeable ZnABs via simple carbonization and activation steps.

Eggplant has high hydrocarbon content (Fig. S1, ESI†) with spongy-like microstructures from interconnected framework of thin cell walls,[9] which is readily converted to low cost porous eggplant carbon (EPC) upon carbonization of its freezedried flesh (cf. ESI† for sample preparation details). As the cell-walls in eggplant possess layered structure with its dimension getting progressively bigger from the external to internal layers,[9] EPCs are obtained as unique 2D sheets of various sizes. The minerals of K, Ca, Mg, Na, etc. that are rich in eggplant (Fig. S1, ESI†) can be washed off, leaving ultrasmall voids to enable high surface area with high population of active sites that further facilitate the electrochemical reactions. At carbonization temperatures (T_c) of 600 to 1000 °C, EPC-T_c are produced. Comparable resistance is found for EPC-900 and EPC-1000, which is much lower than that of EPCs obtained at lower T_c (Fig. S2). Hence, for further investigations in this work EPC-900 with high conductivity yet produced at less stringent condition was used.

EPC-900 was further activated following a modified KOH method[1f, 10] to increase the specific surface area, and the activated product is denoted as A-EPC-900 (cf. ESI† for experimental details). The SEM images show essentially the same morphology as 2D sheets with in-plane size of a few to tens of micrometers and thickness of 100 to 200 nm for all samples (Fig. 1 A–D and Fig. S3, ESI†), suggesting size and shape preservation in the activation. A close-up SEM image in Fig 1B reveals relative smooth surfaces and edges for EPC-900; whereas in contrast A-

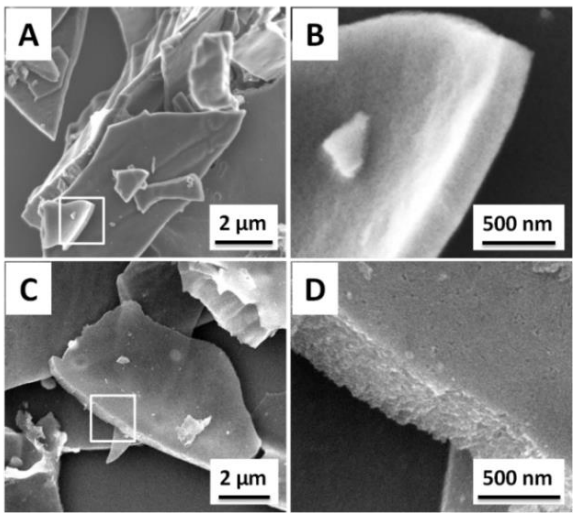

Fig. 1 SEM images of EPC900 before (A and B) and after activation treatment (A-EPC-900, C and D). B) and D) represent the enlarged area as indicated by square in (A) and (C), respectively.

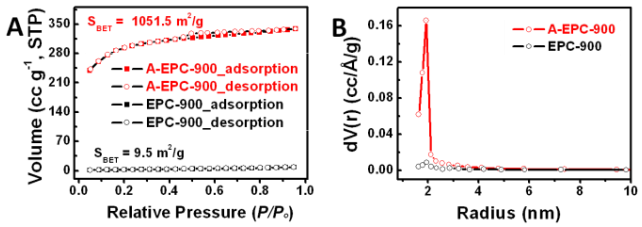

Fig. 2 N_2 adsorption-desorption isotherms (A) and pore size distributions (B) of EPC-900 (black) and A-EPC-900 (red), respectively.

EPC-900 appears much rougher, with numerous distinguishable pore alike features emerged on the surfaces and edges (Fig. 1D and Fig. S4).

The surface area and porosity of EPC-900 and A-EPC-900 were determined using the Brunauer–Emmett–Teller (BET) method, and the results are shown in Fig. 2. Interestingly, the activation process has increased the specific surface area by more than 100-fold, with 1051.5 m^2 g^{-1} for A-EPC-900 as compared to 9.5 m^2 g^{-1} for pristine EPC-900. The characteristic type-IV isotherm curve[4b] of A-EPC-900 suggests the presence of both micro- and mesopore structures. From the Barret-Joyner-Halenda (BJH) plots in Fig. 2B one can see a sharp peak centered at 1.9 nm with a tail into pore size of ~4 nm for A-EPC-900, indicating large volume of microspores with co-existence of mesopores. This makes a clear contrast to the pristine EPC-900, which possesses much smaller populations of both micro- and mesopores (Fig. 2B). Similar small BET surface area and low population of pores were found in EPCs obtained at other carbonization temperatures (Fig. S5). Such 2D micro-sheet structure with high surface area and high population of pores in the size of < 4 nm is of clear structural advantage for A-EPC-900 as a catalyst electrode. With a typical sheet thickness of 100 to 200 nm, majority of its porous structures are readily accessible by both electrolyte and oxygen. The conductive 2D sheets with large in-plane dimension (up to tens of micro-meters) enable efficient electron transfer within the sheets, mitigating unnecessary energy loss due to large contact resistance that typically present in the boundaries of low dimensional and small-sized nanoparticle- or nanowire-based catalysts.

The electrocatalytic activity of A-EPC-900 was investigated and compared with the commercial catalyst Pt/C[5b] (20 wt% Pt on carbon black) and EPC-900 using cyclic voltammetry (CV) and linear sweep voltammetry (LSV) with a rotating disk electrode (RDE). The CV curve gives a cathodic reduction peak at ~ –0.22 V (*vs* Ag/AgCl) as the saturation gas in the electrolyte was switched from N_2 to O_2 (Fig. 3A), suggesting catalytic activity of the materials toward ORR. From the LSV curves obtained at a rotation speed of 1600 rpm for A-EPC-900, EPC-900, bare glassy carbon (GC) electrode and Pt/C (Fig. 3B), one can see that the ORR activity of A-EPC-900 is notably higher. It is also superior to those EPCs obtained by carbonization at other temperatures (Fig. S6). Interestingly, such "metal-free" carbon gives an onset potential of ~ –69 mV which is merely 47 mV more negative than that of Pt/C (–22 mV). Importantly, it delivers higher current (K–L) plots (Fig. 3C) that indicate first-order reaction kinetics against the concentration of dissolved O_2.[5a, 5d] Calculated from the K–L equation,[5a, 5d] the transferred electron number (n) per oxygen

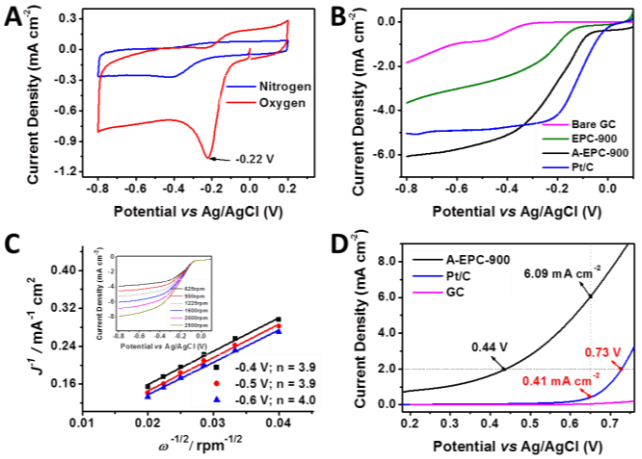

Fig. 3 Electrochemical data of A-EPC-900: A) CV from 0.1M KOH electrolyte, purged by O_2 (red) or N_2 (blue). B) LSV data of A-EPC-900, as compared to GC, EPC-900 and Pt/C for ORR activity at electrode rotating speed of 1600 rpm. C) The Koutecky-Levich plots and fitting data of A-EPC-900 derived from its RDE curves (the insert). D) LSV data of A-EPC-900 as compared to GC, EPC-900 and Pt/C for OER activity. The scan rate was kept at 50m V s^{-1} for CVs and 5 mV s^{-1} for LSV and RDE tests.

molecule in ORR is approximately 4.0 for potential between –0.4 to –0.6 V, suggesting 4-electron transfer behaviour which is an indication of highly efficient ORR catalyst. On the other hand, excellent OER activity of A-EPC-900 is evidenced by its notably less positive onset potential and larger current density as compared to that of the commercial Pt/C at a given potential (Fig. 3D). For instance, at a current density of 2 mA cm^{-2} the potential of A-EPC-900 (0.44 V) is about 290 mV less positive as compared to that of Pt/C (0.73 V); and at a potential of 0.65 V, the current density of A-EPC-900 (6.09 mA cm^{-2}) is ~ 15 times greater than that of Pt/C (0.41 mA cm^{-2}) (Fig. 3D). A-EPC-900 is also found superior to those EPCs obtained at other carbonization temperatures (Fig. S7). Therefore, A-EPC-900 is confirmed as a promising bifunctional oxygen catalyst with ORR comparable to Pt/C, but outperforms Pt/C in OER activity.

To understand the origin of the substantial catalytic activity of A-EPC-900, the compositions of A-EPC-900 and EPC-900 were further studied. In the X-ray diffraction (XRD) patterns of EPC-900 and A-EPC-900 (Fig. 4a), the characteristic (002) and (100) diffraction peaks of carbonaceous materials[8j] are visible for both samples. The *d*- spacing in A-EPC-900 (3.91 Å, 2θ = 22.7°) is slightly smaller than that in EPC-900 (3.95 Å, 2θ = 22.5°), implying higher content of graphitic structure in A-EPC-900 that is likely introduced in the activation process. The Raman spectra (Fig. 4B) support higher content of graphitic structure from EPC-900 to A-EPC-900 with a decreased I_D/I_G value (1.06 → 1.01), the ratio of Raman scattering intensity of the defects induced D–band (1336 cm^{-1}) and the graphitic G–band (1588 cm^{-1}) which is known as an indication of the degree of graphitization of a carbon material.[8a] Moreover, thermogravimetric analysis (TGA) data gives a higher thermal degradation temperature for A-EPC-900 with a new mass loss stage emerged at 700–880 °C (Fig. S8) for the decomposition of high-order graphitic carbons, similar to the one reported previously in CNT.[11]

The residue of EPC-900 likely comprises multiple minerals, as

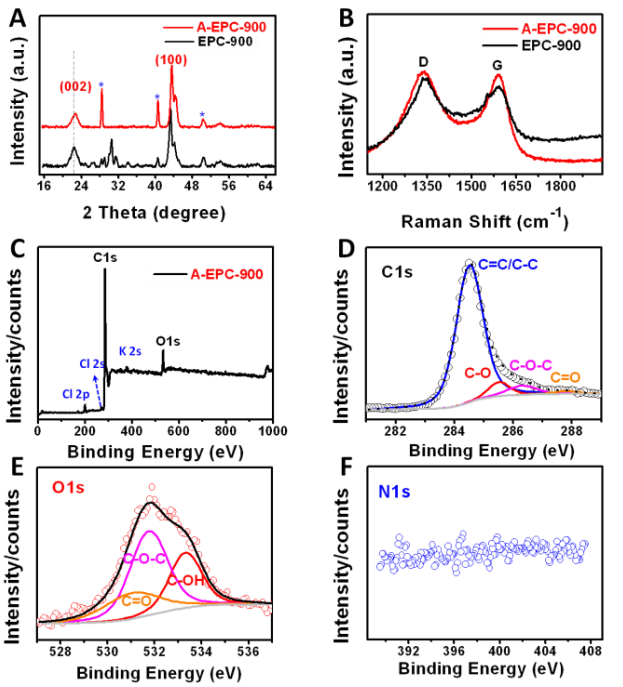

Fig. 4 XRD (A) and Raman (B) spectra of EPC-900 and A-EPC-900. C-F) XPS spectra of A-EPC-900. D-F) show the high resolution C1s, O1s, and N1s spectra, respectively. The Cl 2p (198.9 eV), Cl 2s (270.1 eV) and K 2s (378.0 eV) are attributed to KCl and is consistent with EDX and XRD observations. The absence of Ca, Mg, Na, etc. peaks confirmed that the mineral residues were removed during the activation process.

seen from a series of weak and broad diffraction peaks between the carbon (002) and (100) phases in its XRD pattern (Fig. 4A). As a contrast, a much cleaner XRD pattern is obtained for A-EPC-900, suggesting the removal of minerals in the activation process. The three new emerging peaks can be assigned as (200), (202) and (222) phases of KCl which is likely introduced by the activation process via the reaction of

$$KOH + HCl \rightarrow KCl + H_2O$$

as no Cl was detected in EPC-900 prior to activation according to the Energy dispersive X–ray spectroscopy (EDS) analysis (Fig. S9, S10 and table S1, ESI†). For zinc-air batteries zinc chloride is often added into KOH to form the electrolyte, which makes the presence of small quantity of KCl not a concern in the cathode. Nevertheless, one can still obtain KCl-free EPCs by washing the activated products with hot HCl followed by rinsing with excess amount of DI water, which shows essentially the same ORR and slightly compromised OER catalytic activity (Fig. S11).

It is also worth noting that O is found as the second most abundant element after C in both EPC-900 and A-EPC-900. Elemental mapping on individual carbon sheet reveals that C and O species are homogeneously distributed across the carbon sheets with no detectable N or non-alkaline metal (Fig. S9 and S10, ESI†). In A-EPC-900 the oxygen content is ~ 8.3 wt. %, which equals to a weight ratio of oxygen to carbon (O/C) of 0.11. This value is notably smaller than 0.51 in EPC-900 (Fig. S9, S10, Table S1 in ESI†), suggesting partial removal of oxygen species in the activation treatments which is likely the cause of the decreased *d*-spacing and lower I_D/I_G ratio as observed in A-EPC-900. The presence of oxygen species could facilitate molecular oxygen adsorption on catalyst surfaces thus enhance ORR catalytic activities.[6, 12]

In X-ray photoelectron spectrum (XPS) the strong and sharp peaks at 284.6 eV for C 1s and 531.8 eV for O 1s confirm C and O as the predominant elements in A-EPC-900 (Fig. 4C). The high-resolution spectra and fitting curves of C1s (Fig. 4D) and O1s (Fig. 4E) mainly originate from the functional groups of C-O, O-C-O and C=O.[6, 12] Similar to EPC-900, no clear N signal is distinguishable in the high-resolution N 1s spectrum of A-EPC-900 (Fig. 4F). With the exclusion of contributions by N-doping or noble-metal or transition metal oxides which are known for high performance oxygen electrocatalysts,[2, 5b, 5e] we believe that the high electrocatalytic performance of A-EPC-900 originates from some synergistic effects of the following compositional and/or structural merits: 1) high content of oxygen which likely have created partial positive charge on carbon centres to enhance O_2 adsorption; 2) high content of graphitic structure in large-size 2D sheets with low contact resistance for efficient electron transfer; 3) large surface area with high population of micro pores and active sites on surfaces and edges for smooth electrochemical reactions; 4) ultrathin sheets enabling accessibility of most of the pores and active sites, allowing for fast ion transport and oxygen diffusion. These points are further proven by the results of studies on all EPCs as summarized in Table S2, in which larger surface area and high volume of pores seem beneficial to high electrocatalytic activity, whereas other factors, such as the functionality and chemical composition of EPCs, also have their contributions.

The high ORR and OER catalytic activities of A-EPC-900 are clearly demonstrated by CV and LSV together with RDE tests in 0.1 M KOH which is the typical electrolyte for such studies. In practical ZnABs, however, the concentration of KOH is normally much higher (up to 6-8 M) to achieve high ionic conductivity and inhibit H_2 evolution.[1b,1d,2] At higher concentration of KOH the oxygen solubility is generally lower,[5e] leading to slower ORR and smaller current. This is clearly seen in the CV scans of A-EPC-900, as KOH concentration was increased from 0.1 M to 6 M (Fig. S12). To demonstrate the viability of A-EPC-900 as bifunctional

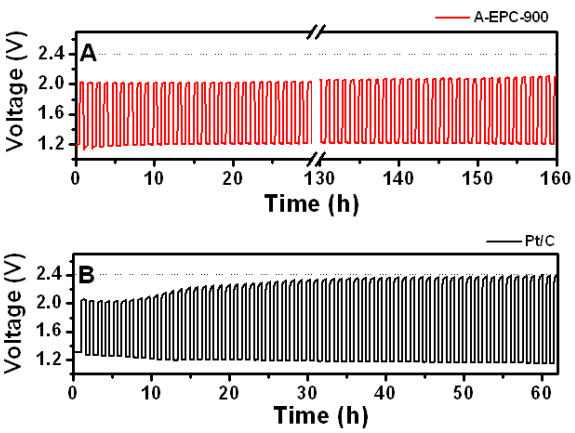

Fig. 5 Zn-Air battery cycling tests data of A) A-EPC-900 based ZnAB at 2 mA cm^{-2}. B) Pt/C-based ZnAB at 2 mA cm^{-2}. One cycle includes 30 min of discharge followed by 30 min of charge.

catalyst in practical batteries, ZnABs were built with A-EPC-900 or Pt/C as the active material in air-cathode, a polished Zn plate as anode, and aqueous solution comprising 6 M KOH and 0.2 M $ZnCl_2$ as electrolyte.[5d] Galvanostatic discharges at current density of 5 mA cm^{-2} gave discharge voltage of 1.23 V at the initial stage for A-EPC-900 based ZnABs (Fig. S13A in ESI†), merely ~10 mV lower than that of its counterpart using Pt/C, which is in good agreement with high ORR performance of A-EPC-900 observed in electrochemical investigations. The specific capacity per gram of consumed Zn (Fig. S13B in ESI†) of ~ 669 mAh g^{-1} for A-EPC-900 based ZnABs is comparable to that of ZnABs in recent reports, built with highly efficient catalysts of CoO/N-CNT[1i] or nanostructured $NiCo_2O_4$.[4c] Cycling tests show little changes in discharge or charge voltages for A-EPC-900 based ZnABs over 160 h and the voltage gap remains at ~ 0.85 V (Fig. 5A). In contrast, Pt/C-based ZnABs require a higher charge potential and its voltage gap quickly increases to ~ 1.25 V, with the charging voltage hitting the cut-off voltage of 2.4 V (at which oxidation of cathode starts to take place) after only 62 h of cycling (Fig. 5B). This clearly proves A-EPC-900 as a more promising catalyst for rechargeable zinc-air batteries.

In summary, microporous carbon sheets with large surface area (1051 m^2 g^{-1}) have been synthesized from a truly renewable and sustainable source, eggplant. High population of active sites on these micro-sheets are readily accessible for ORR and OER, and rich O species on the sheets may facilitate oxygen adsorption and further promote catalytic activities toward ORR and OER. With features of environmental benignity and massive production at low cost, this nature-derived carbon is anticipated to play an important role in the development of large rechargeable Zn-air batteries.

This research was conducted under the project of IMRE/12-2P0504, which is part of the Advanced Energy Storage Research Programme, supported by Science and Engineering Research Council (SERC) of A*STAR (Agency for Science, Technology and Research), Singapore.

Notes and references

[a]*Institute of Materials Research and Engineering, A*STAR (Agency for Science, Technology and Research), 3 Research Link, Singapore 117602, Republic of Singapore*
E-mails: zl-liu@imre.a-star.edu.sg (Z.L. Liu); y-zong@imre.a-star.edu.sg (Y. Zong)
[b]*National Junior College, 37 Hillcrestate Road, Singapore 288913, Republic of Singapore*
[c]*Department of Chemistry, National University of Singapore, 3 Science Drive 3, Singapore 117543, Republic of Singapore*
E-mail: andyhor@nus.edu.sg (T.S.A. Hor)
[#] *The authors contributed equally to this work*

† Electronic Supplementary Information (ESI) available: Experimental 700details; SEM images of EPC-700, EPC-800 and EPC-1000; TGA, LSV and EDX results of EPCs. See DOI: 10.1039/b000000x/

1 (a) M. A. Rahman, X. Wang and C. Wen, *J. Electrochem. Soc*., 2013, **160**, A1759; (b) Y. Li and H. Dai, *Chem. Soc. Rev.*, 2014, **43**, 5257; (c) K. Gong, F. Du, Z. Xia, M. Durstock and L. Dai, *Science*, 2009, **323**, 760; (d) F. Cheng and J. Chen, *Chem. Soc. Rev.*, 2012, **41**, 2172; (e) T. Yu, J. Jiang, J. Zhu, W. Ai, Z. Fan, H. Zhang, J. Liu, X. Shen and C. Zou, *Energy Environ. Sci.*, 2014, **7**, 2670; (f) Y. Zhu, S. Murali, M. D. Stoller, K. J. Ganesh, W. Cai, P. J. Ferreira, A. Pirkle, R. M. Wallace, K. A. Cychosz, M. Thommes, D. Su, E. A. Stach and R. S. Ruoff, *Science*, 2011, **332**, 1537; (g) M. Park, J. Ryu, Y. Kim and J. Cho, *Energy Environ. Sci.*, 2014, **7**, 3727; (h) Y. Li, P. Hasin and Y. Wu, *Adv. Mater*., 2010, **22**, 1926; (i) Y. Li, M. Gong, Y. Liang, J. Feng, J.-E. Kim, H. Wang, G. Hong, B. Zhang and H. Dai, *Nat. Commun*, 2013, **4**, 1805. (j) Y. Xu, X. Zhu, X. Zhou, X. Liu, Y. Liu, Z. Dai and J. Bao, *J. Phys. Chem. C*, 2014, **118**, 28502; (k) X. Liu, Y. Du, L. Hu, X. Zhou, Y. Li, Z. Dai and J. Bao, *J. Phys. Chem. C*, 2015, **119**, 5848.

2 J.-S. Lee, S. T. Kim, R. Cao, N.-S. Choi, M. Liu, K. T. Lee and J. Cho, *Adv. Energy Mater.*, 2011, **1**, 34.

3 (a) A. Morozan, B. Jousselme and S. Palacin, *Energy Environ. Sci.*, 2011, **4**, 1238; (b) C. Zhu and S. Dong, *Nanoscale*, 2013, **5**, 10765.

4 (a) F. Cheng, J. Shen, B. Peng, Y. Pan, Z. Tao and J. Chen, *Nat. Chem*, 2011, **3**, 79; (b) Y. Su, Y. Zhu, H. Jiang, J. Shen, X. Yang, W. Zou, J. Chen and C. Li, *Nanoscale*, 2014, **6**, 15080; (c) M. Prabu, K. Ketpang and S. Shanmugam, *Nanoscale*, 2014, **6**, 3173.

5 (a) Y. Liang, Y. Li, H. Wang, J. Zhou, J. Wang, T. Regier and H. Dai, *Nat. Mater.*, 2011, **10**, 780; (b) Y. Li, W. Zhou, H. Wang, L. Xie, Y. Liang, F. Wei, J.-C. Idrobo, S. J. Pennycook and H. Dai, *Nat. Nanotechnol.*, 2012, **7**, 394; (c) G. Zhang, B. Y. Xia, X. Wang and X. W. Lou, *Adv. Mater.*, 2014, **26**, 2408; (d) B. Li, X. Ge, F. W. T. Goh, T. S. A. Hor, D. Geng, G. Du, Z. Liu, J. Zhang, X. Liu and Y. Zong, *Nanoscale*, 2015, **7**, 1830; (e) J.-S. Lee, G. S. Park, H. I. Lee, S. T. Kim, R. Cao, M. Liu and J. Cho, *Nano Lett.*, 2011, **11**, 5362.

6 R. Silva, D. Voiry, M. Chhowalla and T. Asefa, *J. Am. Chem. Soc.*, 2013, **135**, 7823.

7 (a) L. Qu, Y. Liu, J.-B. Baek and L. Dai, *ACS Nano*, 2010, **4**, 1321; (b) L. Chen, R. Du, J. Zhu, Y. Mao, C. Xue, N. Zhang, Y. Hou, J. Zhang and T. Yi, *Small*, 2015, **11**, 1423; (c) D. S. Geng, N. Ding, T. S. A. Hor, Z. L. Liu, X. L. Sun and Y. Zong, *J. Mater. Chem. A*, 2015, **3**, 1795; (d) J. T. Zhang, Z. H. Zhao, Z. H. Xia and L. M. Dai, *Nat. Nanotechnol*., 2015, DOI: 10.1038/nnano.2015.48.

8 (a) E. M. Lotfabad, J. Ding, K. Cui, A. Kohandehghan, W. P. Kalisvaart, M. Hazelton and D. Mitlin, *ACS Nano*, 2014, **8**, 7115; (b) S. Gao, H. Fan, Y. Chen, L. Li, Y. Bando and D. Golberg, *Nano Energy*, 2013, **2**, 1261; (c) C. Zhu, J. Zhai and S. Dong, *Chem. Commun.*, 2012, **48**, 9367; (d) E. Unur, *Micropor. Mesopor. Mater.*, 2013, **168**, 92; (e) S. Liu, J. Tian, L. Wang, Y. Zhang, X. Qin, Y. Luo, A. M. Asiri, A. O. Al-Youbi and X. Sun, *Adv. Mater.*, 2012, **24**, 2037; (f) L. Zhu, Y. Yin, C.-F. Wang and S. Chen, *J. Mater. Chem. C*, 2013, **1**, 4925; (g) J. Ding, H. Wang, Z. Li, K. Cui, D. Karpuzov, X. Tan, A. Kohandehghan and D. Mitlin, *Energy Environ. Sci*., 2015, **8**, 941; (h) S. Gao, Y. Chen, H. Fan, X. Wei, C. Hu, H. Luo and L. Qu, *J. Mater. Chem. A*, 2014, **2**, 3317; (i) H. Zhu, X. Wang, F. Yang and X. Yang, *Adv. Mater.*, 2011, **23**, 2745; (j) J. Ding, H. Wang, Z. Li, A. Kohandehghan, K. Cui, Z. Xu, B. Zahiri, X. Tan, E. M. Lotfabad, B. C. Olsen and D. Mitlin, *ACS Nano*, 2013, **7**, 11004.

9 A. Puig, I. Perez-Munuera, J. A. Carcel, I. Hernando and J. V. Garcia-Perez, *Food Bioprod. Process.*, 2012, **90**, 624.

10 L. Qie, W. Chen, H. Xu, X. Xiong, Y. Jiang, F. Zou, X. Hu, Y. Xin, Z. Zhang and Y. Huang, *Energy Environ. Sci.*, 2013, **6**, 2497.

11 I. H. Hafez, M. R. Berber, T. Fujigaya and N. Nakashima, *Sci. Rep.*, 2014, **4**, 6295.

12 S. Wang, S. Dong, J. Wang, L. Zhang, P. Han, C. Zhang, X. Wang, K. Zhang, Z. Lan and G. Cui, *J. Mater. Chem.*, 2012, **22**, 21051.